chemosensors

MDPI

Article

Mechanism of Fast NO Response in a WO_3-Nanorod-Based Gas Sensor

Giacometta Mineo [1,2], Kaveh Moulaee [3], Giovanni Neri [3], Salvo Mirabella [1,2,*] and Elena Bruno [1,2]

[1] Dipartimento di Fisica e Astronomia "Ettore Majorana", Università degli Studi di Catania, Via S. Sofia 64, 95123 Catania, Italy
[2] CNR-IMM, Università di Catania, Via S. Sofia 64, 95123 Catania, Italy
[3] Dipartimento di Ingegneria, Università degli Studi di Messina, Contrada Di Dio, Sant'Agata, 98158 Messina, Italy
* Correspondence: salvo.mirabella@dfa.unict.it

Abstract: The development of fast and reliable gas sensors is a pressing and growing problem for environmental monitoring due to the presence of pollutants in the atmosphere. Among all gases, particular attention is devoted to NO, which can cause serious health problems. WO_3 nanorods represent promising candidates for this purpose due to their high electrical stability and low cost of production. Here, the hydrothermal synthesis of WO_3 nanorods is reported, in addition to the realization of a chemo-resistive NO sensor. NO-sensing tests were performed at different temperatures (250–400 °C) and under different gas concentrations (250–2500 ppm), and NO response and recovery curves were also modeled by using the Langmuir adsorption theory by highlighting the NO-sensing mechanism of the WO_3 nanorods. An interaction occurred at the surface between NO and the adsorbed oxygen ions, thus clarifying the NO-reducing behavior. The fast response and recovery times open the route for the development of fast NO sensors based on WO_3.

Keywords: gas sensor; nitric oxide; tungsten oxide; nanostructures; chemo-resistive effect

Citation: Mineo, G.; Moulaee, K.; Neri, G.; Mirabella, S.; Bruno, E. Mechanism of Fast NO Response in a WO_3-Nanorod-Based Gas Sensor. *Chemosensors* **2022**, *10*, 492. https://doi.org/10.3390/chemosensors10110492

Academic Editor: Manuel Aleixandre

Received: 11 October 2022
Accepted: 18 November 2022
Published: 20 November 2022

1. Introduction

Nitric oxide (NO) is an odorless and colorless gas that is largely produced in urban areas as exhaust gas from gas stoves and motor vehicles, as well as in high-temperature combustion and industrial processes. Serious health problems, such as respiratory diseases and skin and eye irritations, can be caused by exposure to even low concentrations of NO. Moreover, high concentrations of NO can cause acidic rains, the production of ozone, and photochemical smog [1,2]. Therefore, fast and very sensitive devices are demanded for the detection of NO in order to bring it under control and even reduce its harmful effects on humans and other beings in the environment.

Due to nanotechnology, great strides have been made in sensitivity with the realization of NO chemo-sensors with a very low limit of detection of about 10 ppm [3–6], which is below the Immediately Dangerous to Life or Health (IDLH) value (100 ppm) and the Threshold Limit Value (TLV, 25 ppm) [7]. Nonetheless, their response time, which is still higher than 50–60 s, still represents an important limit in their use [5,6].

Nanostructured semiconductors, such as CuO [1], TiO2 [8], MoS_2 [9], La_2O_3 [10], and WO_3 [11], have been extensively used for the development of NO gas sensors, and the 1D morphology (nanorods, nanowires, and nanotubes) seems to be the best way to achieve a high sensitivity and low limit of detection (LoD) due to the high surface-to-volume ratio [12]. Among them, WO_3 represents one of the most suitable candidates for the development of many gas sensors, such as ethanol sensors [13], H_2S sensors [14], C_2H_2 sensors [15], and NO sensors [11]. It is an *n*-type semiconductor with an indirect band gap ranging between 2.4 and 2.8 eV [16]; it has a high performance in terms of sensitivity and is promising in terms of rapidity due to its high versatility and stability, and the possibility

of easily synthesizing 1D nanostructures, such as nanorods. Cai et al. [11] synthesized WO_3 nanowires by using hydrothermal synthesis, and their NO-sensing tests showed a good response towards 500 ppm of NO at 300 °C with an interesting response time of 63 s. The addition of noble metals improved the sensing activity with a good reduction of the response time, as confirmed by many theoretical studies [17,18]. Chen et al. [3] synthesized WO_3 nanoplates that were decorated with silver nanoparticles, which showed a response time of 20 s for NO at 0.5–100 ppm with an operating temperature of 170 °C; Cai et al. [4] synthesized hierarchical Pd-decorated flowerlike WO_3 nanostructures by using the solvothermal method; these were tested for their NO-sensing ability as a function of the Pd amount, and they delivered a high response to 20 ppm of NO at 200 °C with a response time of about 30 s. Unfortunately, the use of noble metals increases the production costs of the sensors, so WO_3 nanostructures need some optimizations in order to improve their sensitivity and rapidity without using noble metals. To achieve this goal, a comprehensive understanding of the interaction between WO_3 and NO based on experimental results is necessary, but this is still missing. A step forward in the understanding of NO sensing with WO_3 can be achieved through a basic comprehension of the actual processes underlying the WO_3–NO interaction, allowing one to obtain a high-performance WO_3-based NO sensor.

In this paper, we synthesized hexagonal WO_3 nanorods by using a hydrothermal technique and studied the interactions with NO molecules at different temperatures and concentrations. The experimental kinetic response and recovery curves of the WO_3 nanorods were modeled by using the Langmuir adsorption theory, allowing the identification of the thermally activated processes that occurred and their characteristic times, which showed a chemo-resistive effect. A comprehensive description of the NO–WO_3 interaction based on the experimental curves is discussed, in addition to the determination of the response and recovery times.

2. Materials and Methods

Hexagonal WO_3 nanorods were synthesized through hydrothermal synthesis, and the precursor solution was prepared by using sodium tungstate (Na_2WO_2), sodium chloride (NaCl), and hydrochloric acid (HCl). The thermal treatment was performed at 180 °C for 3 h; the obtained powders were collected and washed by using deionized water and ethanol and dried on a hot plate in air at 50 °C for 1 h [19]. The obtained powders were dissolved in deionized water with a concentration ratio of 1:4, and some drops of the WO_3-based solution were released on a conductometric gas sensor, which consisted of an alumina substrate (6×3 mm^2) with a Pt heather on the backside and interdigitated Pt electrodes on the front side (inset in Figure 1b). Morphological analyses were carried out by using a scanning electron microscope (SEM; Gemini Field Emission SEM Carl Zeiss SUPRATM 25 (FEG-SEM, Carl Zeiss Microscopy GmbH, Jena, Germany)). NO-gas-sensing measurements were performed in a stainless-steel test chamber that allowed measurements in a controlled atmosphere. NO gas was used and diluted in synthetic dry air at a given concentration by using mass-flow controllers. The sensor was heated from room temperature (∼20 °C) up to 400 °C in dry synthetic air with a relative humidity (RH) lower than 3% by using a dual-channel power-supplier instrument (Agilent E3632A) to bias the built-in heater. The response to NO gas was evaluated by recording the resistance at an applied voltage of 1.0 V through a Keithley 6487 picometer with a time step of about 2.5 s.

The analysis of the experimental curves provided information about the kinetics of the NO sensing in the approximation of a monolayer adsorption onto a homogeneous surface. Starting from the assumptions that there were not phase transitions and that the adsorption took place at specific localized sites that could accommodate only one NO molecule, the Langmuir adsorption theory allowed us to study the sensor's reactions during the response phase, S, and the recovery phase, S^*, by fitting the experimental response and recovery curves through the consideration of one ($w = 1$) or two ($w \neq 1$) isotherm equations, depending on the number of active reaction channels, as follows [20,21]:

$$S = S_0\{w[1 - exp(-t/\tau_1)] + (1 - w)[1 - exp(-t/\tau_2]\} \quad (1)$$

$$S^* = S_0[w^* * exp(-t/\tau_1^*) + (1 - w^*) * exp(-t/\tau_2^*)] \quad (2)$$

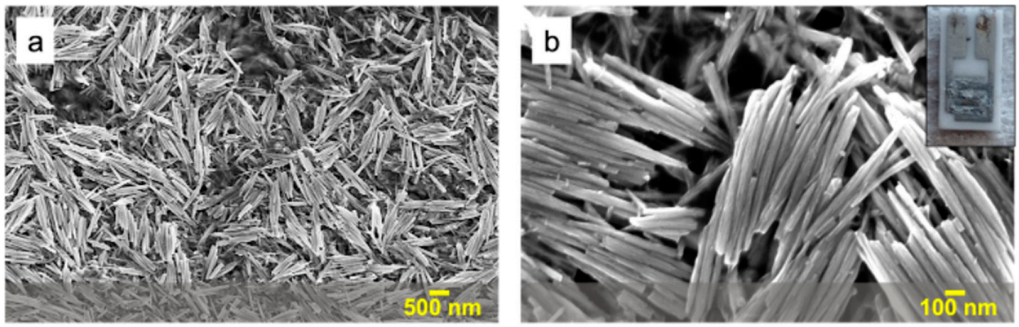

Figure 1. Low- (**a**) and high-magnification (**b**) SEM images of WO_3 nanorods deposited onto an interdigitated electrode (inset).

In these equations, S_0 is the maximum value of the change in resistance (the same value was fixed for the response and recovery phases), τ_n and τ_n^* (n stands for 1 or 2) are lifetimes associated with the two isotherms during the response and recovery phases, respectively, and w and w^* are weights attributed to reaction channel 1 during the response and recovery phases, respectively.

3. Results and Discussion

3.1. Morphological Results

Figure 1a,b show the low- and high-magnification SEM images of the hydrothermally synthesized WO_3 nanorods, which had an average length and diameter of about 700 nm and 50 nm, respectively, and were drop-coated on the conductometric gas sensor to cover all of the electrical contacts in order to maximize the electrical signal (inset in Figure 1b). Our previous work confirmed the hexagonal crystal structure for WO_3 nanorods prepared under similar conditions [19].

3.2. NO-Sensing Measurements

Experimental NO-sensing curves were obtained by considering the variations in the resistance as a function of time while a mixture of NO and dry air or only dry air were fluxed into the test chamber (response and recovery phase, respectively). Different temperatures in the range of 250–400 °C were tested. A sensor response towards NO appeared at 350 °C, and different NO concentrations (250–2500 ppm) were evaluated. Figure 2 shows the variations in the resistance (black curve) under cycles of different NO concentrations (red curve) at 350 °C; the resistance decreased when NO gas was fluxed into the test chamber (purple arrow) and increased when the NO flux was stopped (yellow arrow).

Such a response of the sensor under an NO-rich atmosphere allows us to define the sensor response S(%) as follows:

$$S(\%) = \left(R_a - R_g\right)/R_a * 100 \quad (3)$$

in which R_g and R_a are the measured resistances in the presence and absence of NO gas, respectively. To understand the WO_3–NO interaction, S(%) is defined as a function of the temperature and concentration. Figure 3 shows the values of S(%) obtained at different temperatures (black squares) of (a) 250, (b) 300, and (c) 350 °C under a 500 ppm flux of NO as a function of elapsed time during the response and recovery phases (defined according to Figure 2). The response curves rapidly increased when NO was fluxed into the test chamber and tended to saturate within 30 s. After the NO flux was stopped, the recovery curves decreased with a temperature-dependent trend. S(%) was higher at lower temperatures, but the recovery mechanism was not very efficient. NO concentration tests were carried out at 350 °C to maximize the recovery mechanism. Figure 4 shows the S(%) values (black squares)

obtained under different NO concentrations of (a) 250, (b) 500, (c) 1000, and (d) 2500 ppm at 350 °C.

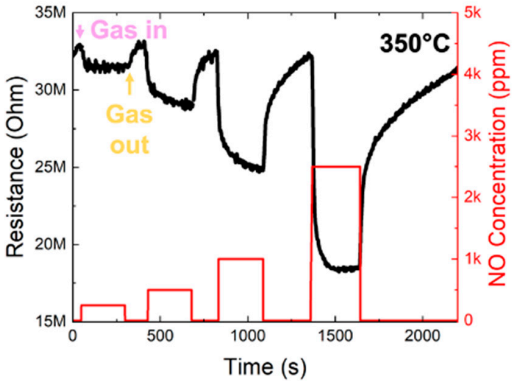

Figure 2. Dynamic resistance variations of the WO_3-based sensor (black curve) at 350 °C under cycles of different NO concentrations (red curve). The arrows indicate when NO was fluxed into the chamber (named "gas in") or it was stopped (named "gas out"), which coincided with the start of the response and the recovery phases, respectively.

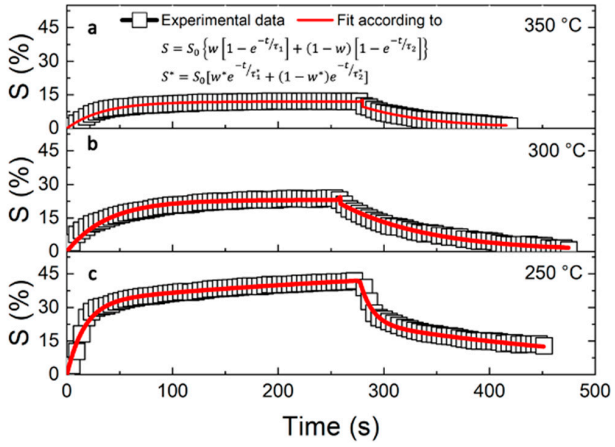

Figure 3. Dynamic responses of the WO_3-based sensor (squared symbols) and the fit (red lines) obtained at (**a**) 350, (**b**) 300, and (**c**) 250 °C under 500 ppm of NO as a function of elapsed time, starting when NO was fluxed into the chamber.

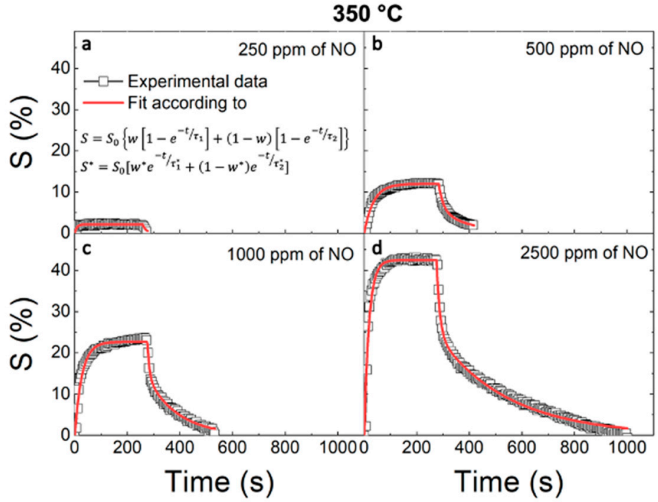

Figure 4. Dynamic responses of the WO_3-based sensor (squared symbols) and the fit (red lines) obtained at 350 °C under (**a**) 250, (**b**) 500, (**c**) 1000, and (**d**) 2500 ppm fluxes of NO as a function of elapsed time.

The response curves increased when NO was fluxed into the test chamber, and again, they tended toward saturation after 30 s. After the NO flux was stopped, the recovery curves decreased and tended toward the initial value, as expected. Higher NO concentrations resulted in a greater response. Additionally, for higher concentrations of NO, the recovery phase was prolonged, as it required a longer time for a full recovery of the sensor after exposure to the target NO gas.

3.3. NO-Sensing Mechanism

The kinetics of the NO sensing could be determined from the analysis of the experimental curves by considering the Langmuir adsorption theory [20] and according to Equations (1) and (2) that were reported in Section 2 (by fixing $w = 1$ in most cases) for the response and recovery phases, respectively. The fitting curves (red lines) shown in Figures 3 and 4 reproduced the obtained experimental data (black squares) well, thus confirming that only one reaction channel was active during most of the response phases (only one isotherm was used, $w = 1$), while during the recovery phase, a fast (R1) and a slow (R2) reaction channel, independently and concomitantly, were active (two isotherms were used, $w \neq 1$). The fitting parameters as a function of temperature are listed in Table 1. The maximum response S_0 strongly depended on the temperature; it reached its maximum (53%) at 250 °C and decreased to 12% at 350 °C, as expected from the experimental curves. At 250 °C, during the response and recovery phases, both R1 and R2 were active, unlike what happened at 300 and 350 °C, where only R1 was active. R1 was characterized by typical times of a few seconds (5–40 s), while R2 was characterized by long times in both the response (~460 s) and the recovery phase (~290 s). Concerning the weight w, it was 0.6 and 0.4 for the response and recovery phases, respectively. These results confirm that at 350 °C, the sensor possessed the lowest response times, which are competitive with those reported for noble-metal-decorated sensors, which are about 20 s for Ag-decorated WO_3 nanoparticles [3] and about 30 s for Pd-decorated WO_3 nanoflowers [4], despite the lowest response being towards 500 ppm of NO, thus further justifying the choice of this temperature for the sensing tests with different NO concentrations and, thus, opening the route to further improvements in the performance of the sensor.

Table 1. Results of the fitting procedure for the response and recovery transients at various temperatures and a fixed concentration of NO (500 ppm).

Temperature (°C)	S_0 **(%)**	τ_1 **(s)**	τ_2 **(s)**	w **(%)**	τ_1^* **(s)**	τ_2^* **(s)**	w^* **(%)**
250	53	17	461	0.6	12	288	0.5
300	23	39	-	-	7	93	0.8
350	12	35	-		17	121	0.6

An analogous analysis was carried out at a fixed temperature by varying the NO concentration. Experimental curves were fitted in accordance with Equations (1) and (2) (red curves in Figure 4); an excellent agreement was obtained, as mentioned above, and the obtained fitting parameters are reported in Table 2. During the response phase, only one process was active ($w = 1$) under 250 and 500 ppm of NO flux, with surprisingly low characteristic times of the order of 10–40 s, as well as for the correlated recovery phase. In the other cases, the response and recovery phases were characterized by the activation of two mechanisms, R1 and R2, with very short (10–35 s) and long (110–280 s) times, respectively. S_0 increased with the increase in NO concentration, as expected, with the maximum value (43%) being at 2500 ppm.

Table 2. Results of the fitting procedure for the response and recovery transients with various concentrations of NO at the temperature of 350 °C.

Concentration (ppm)	S_0 (%)	τ_1 (s)	τ_2 (s)	w (%)	τ_1^* (s)	τ_2^* (s)	w^* (%)
250	2	8	-	-	14	-	-
500	12	35	-	-	67	-	-
1000	26	20	254	0.8	8	117	0.4
2500	43	18	103	0.9	13	272	0.4

The NO–WO_3 interactions can be described by starting from the results of Langmuir-based modeling [1,19,20], which allowed us to identify the chemical reaction occurring during the NO-sensing mechanism; this was dominated by reducing processes, since WO_3 is an *n*-type semiconductor and the electrical resistance decreased after exposure to NO. Gas-sensing measurements were carried out in a controlled atmosphere, in which the O_2 concentration was kept constant during the response and recovery phases. This resulted in a high concentration of oxygen ions on the surface of WO_3, whereby our experimental data suggested an interaction between the NO molecules and the oxygen adsorbed onto the WO_3 surface, rather than a direct interaction with the WO_3. According to the literature [1], the interaction between NO and adsorbed oxygen occurs as follows:

$$NO + O_{ads}^{2-} -> NO_2 + 2e^-$$

$$NO + O_{ads}^{-} -> NO_2 + e^-$$

which results in a decrease in electrical resistance according to the experimental data. At 250 °C, both chemical reactions occurred, thus leading to the activation of both R1 and R2, while in the other cases, only the first occurred, since O_{ads}^{2-} is the most stable ion at temperatures higher than 300 °C. No response toward 500 ppm of NO was obtained at 400 °C. This experimental evidence and the decrease in S_0 with the increase in the temperature suggest a quenching of the interaction between NO and adsorbed oxygen with increasing temperature.

The recovery phase occurred through the interaction between the O_2 present in the dry synthetic air and the surface of WO_3 by restoring the initial conditions. R1 and R2 could arise from the O_2 molecules adsorbed onto the WO_3 surface in the form of O_{ads}^- and O_{ads}^{2-}, respectively, as follows [22]:

$$O_{2\ ads}^- + e^- \rightarrow 2O_{ads}^- \text{ if } 100^\circ C < T < 300\ ^\circ C$$

$$O_{ads}^- + e^- \rightarrow O_{ads}^{2-} \text{ if } T > 300\ ^\circ C$$

At 250 °C, the recovery phase occurred through the activation of only R1, since O_{ads}^{2-} does not exist at this temperature. At 350 °C, high NO concentrations (1000 and 2500 ppm) quickly ran out of $O_{(ads)}^{2-}$ reserves (R1), whereby the interaction occurred with few $O_{(ads)}^{2-}$ (the low concentration was due to the high temperature).

4. Conclusions

A powder of noble metal-free WO_3 nanorods (400 nm long, 50 nm large) was produced by using a hydrothermal technique and then drop-casted onto interdigitated Pt electrodes, which were used to analyze the WO_3–NO interaction after exposure to different concentrations (250–2500 ppm) at different temperatures (250–400 °C). The experimental data show a trend that suggests that the interaction occurred through reducing processes. The Langmuir adsorption theory was successfully used to model the experimental data by individuating two interaction channels and their characteristic times between the NO and the adsorbed oxygen species on the WO_3 surface, whose activation depended on the temperature. The fast and slow channels were attributed to the interactions between NO and O_{ads}^{2-} and O_{ads}^-, respectively, with lifetimes of the order of a few seconds in the first case and of the order of

≈450 s in the latter case. The recovery phase was dominated by the adsorption of O onto the WO_3 surface in the form of O^-_{ads} and O^{2-}_{ads}, with lifetimes of a few seconds in the first case and of 100–300 s in the second case. The fastest processes dominated the response and the recovery phases, thus speeding up the sensing performance, which was comparable with that reported in the literature for noble-metal-decorated sensors. The higher response at low temperatures can open the route to the development of free-Pt WO_3-based NO sensors with low operating temperatures and low response times.

Author Contributions: Conceptualization, G.M., K.M., G.N., S.M. and E.B.; Data curation, G.M., K.M., G.N., S.M. and E.B.; Formal analysis, G.M.; Investigation, G.M. and K.M.; Methodology, G.M. and K.M.; Supervision, K.M., G.N., S.M. and E.B.; Writing—Original draft, G.M.; Writing—Review and editing, K.M., G.N., S.M. and E.B. All authors have read and agreed to the published version of the manuscript.

Funding: This work was supported by PON MIUR ADAS +: ARS01_00459, by programma di ricerca di Ateneo UNICT 2020-22 linea 2 PIA.CE.RI "NaTI4Smart Sviluppo di Nanomateriali e Tecnologie Innovative per Smart detection", by PRIN 2017 CLEAN-Valorizing Sustainable Plastics through a CLEver use of NANoparticles: 20174FSRZS_003, by Progetto ARS01_00345-4FRAILTY-Sensoristica intelligente, infrastrutture e modelli gestionali per la sicurezza di soggetti fragili, and by European Union (NextGeneration EU), through the MUR-PNRR project SAMOTHRACE (ECS00000022).

Institutional Review Board Statement: Not applicable.

Informed Consent Statement: Not applicable.

Data Availability Statement: The data presented in this study are available on request from the corresponding author.

Acknowledgments: The authors wish to thank G. Pantè, C. Percolla, and S. Tatì (CNR-IMM Catania, Italy) for their technical support, in addition to the Service Center B.R.I.T. of University of Catania.

Conflicts of Interest: The authors declare no conflict of interest.

References

1. Censabella, M.; Iacono, V.; Scandurra, A.; Moulaee, K.; Neri, G.; Ruffino, F.; Mirabella, S. Low Temperature Detection of Nitric Oxide by CuO Nanoparticles Synthesized by Pulsed Laser Ablation. *Sens. Actuators B Chem.* **2022**, *358*, 131489. [CrossRef]
2. Tao, P.; Xu, Y.; Zhou, Y.; Song, C.; Qiu, Y.; Dong, W.; Zhang, M.; Shao, M. Nitrogen Oxide (NO) Gas-Sensing Properties of Bi_2MoO_6 Nanosheets Synthesized by a Hydrothermal Method. *Mater. Res.* **2017**, *20*, 786–790. [CrossRef]
3. Chen, D.; Yin, L.; Ge, L.; Fan, B.; Zhang, R.; Sun, J.; Shao, G. Low-Temperature and Highly Selective NO-Sensing Performance of WO_3 Nanoplates Decorated with Silver Nanoparticles. *Sens. Actuators B Chem.* **2013**, *185*, 445–455. [CrossRef]
4. Cai, Z.X.; Li, H.Y.; Ding, J.C.; Guo, X. Hierarchical Flowerlike WO_3 Nanostructures Assembled by Porous Nanoflakes for Enhanced NO Gas Sensing. *Sens. Actuators B Chem.* **2017**, *246*, 225–234. [CrossRef]
5. Wu, M.R.; Li, W.Z.; Tung, C.Y.; Huang, C.Y.; Chiang, Y.H.; Liu, P.L.; Horng, R.H. NO Gas Sensor Based on $ZnGa_2O_4$ Epilayer Grown by Metalorganic Chemical Vapor Deposition. *Sci. Rep.* **2019**, *9*, 7459. [CrossRef] [PubMed]
6. Samanta, C.; Ghatak, A.; Raychaudhuri, A.K.; Ghosh, B. ZnO/Si Nanowires Heterojunction Array-Based Nitric Oxide (NO) Gas Sensor with Noise-Limited Detectivity Approaching 10 Ppb. *Nanotechnology* **2019**, *30*, 305501. [CrossRef]
7. Available online: https://www.cdc.gov/niosh/npg/npgd0448.html (accessed on 2 November 2022).
8. Murali, G.; Reddeppa, M.; Seshendra Reddy, C.; Park, S.; Chandrakalavathi, T.; Kim, M.D.; In, I. Enhancing the Charge Carrier Separation and Transport via Nitrogen-Doped Graphene Quantum Dot-TiO_2 Nanoplate Hybrid Structure for an Efficient NO Gas Sensor. *ACS Appl. Mater. Interfaces* **2020**, *12*, 13428–13436. [CrossRef]
9. Ramu, S.; Chandrakalavathi, T.; Murali, G.; Kumar, K.S.; Sudharani, A.; Ramanadha, M.; Peta, K.R.; Jeyalakshmi, R.; Vijayalakshmi, R.P. UV Enhanced NO Gas Sensing Properties of the MoS_2 Monolayer Gas Sensor. *Mater. Res. Express* **2019**, *6*, 085075. [CrossRef]
10. Yadav, A.A.; Lokhande, A.C.; Kim, J.H.; Lokhande, C.D. Improvement in CO_2 Sensing Characteristics Using Pd Nanoparticles Decorated La_2O_3 Thin Films. *J. Ind. Eng. Chem.* **2017**, *49*, 76–81. [CrossRef]
11. Cai, Z.X.; Li, H.Y.; Yang, X.N.; Guo, X. NO Sensing by Single Crystalline WO_3 Nanowires. *Sens. Actuators B Chem.* **2015**, *219*, 346–353. [CrossRef]
12. Moon, H.G.; Choi, Y.R.; Shim, Y.S.; Choi, K.I.; Lee, J.H.; Kim, J.S.; Yoon, S.J.; Park, H.H.; Kang, C.Y.; Jang, H.W. Extremely Sensitive and Selective NO Probe Based on Villi-like WO_3 Nanostructures for Application to Exhaled Breath Analyzers. *ACS Appl. Mater. Interfaces* **2013**, *5*, 10591–10596. [CrossRef] [PubMed]
13. Wei, Z.; Zhou, Q.; Wang, J.; Zeng, W. Hydrothermal Synthesis of Hierarchical WO_3/NiO Porous Microsphere with Enhanced Gas Sensing Performances. *Mater. Lett.* **2020**, *264*, 127383. [CrossRef]

14. Wei, Z.; Zhou, Q.; Zeng, W. Hierarchical WO_3–NiO microflower for high sensitivity detection of SF_6 decomposition byproduct H_2S. *Nanotechnology* **2020**, *31*, 215701. [CrossRef] [PubMed]
15. Wei, Z.; Zhou, Q.; Lu, Z.; Xu, L.; Gui, Y.; Tang, C. Morphology Controllable Synthesis of Hierarchical WO_3 Nanostructures and C_2H_2 Sensing Properties. *Phys. E Low Dimens. Syst. Nanostruct.* **2019**, *109*, 253–260. [CrossRef]
16. Yadav, A.A.; Hunge, Y.M.; Kang, S.W. Porous Nanoplate-like Tungsten Trioxide/Reduced Graphene Oxide Catalyst for Sonocatalytic Degradation and Photocatalytic Hydrogen Production. *Surf. Interfaces* **2021**, *24*, 101075. [CrossRef]
17. Li, Z.; Jia, L.; Chen, J.; Cui, X.; Zhou, Q. Adsorption and Sensing Performances of Pristine and Au-Decorated Gallium Nitride Monolayer to Noxious Gas Molecules: A DFT Investigation. *Front. Chem.* **2022**, *10*, 898154. [CrossRef]
18. Peng, R.; Zhou, Q.; Zeng, W. First-Principles Insight into Pd-Doped C_3N Monolayer as a Promising Scavenger for NO, NO_2 and SO_2. *Nanomaterials* **2021**, *11*, 1267. [CrossRef]
19. Mineo, G.; Moulaee, K.; Neri, G.; Mirabella, S.; Bruno, E. H_2 Detection Mechanism in Chemoresistive Sensor Based on Low-Cost Synthesized WO_3 Nanorods. *Sens. Actuators B Chem.* **2021**, *348*, 130704. [CrossRef]
20. Urso, M.; Gianluca, S.; Neri, G.; Petralia, S.; Conoci, S.; Priolo, F.; Mirabella, S. Sensors and Actuators B: Chemical Room Temperature Detection and Modelling of Sub-Ppm NO_2 by Low-Cost Nanoporous NiO Fi Lm. *Sens. Actuators B Chem.* **2020**, *305*, 127481. [CrossRef]
21. Czepirski, L.; Balys, M.R.; Komorowska-Czepirska, E. Some generalization of Langmuir adsorption isotherm. *Internet J. Chem.* **2000**, *3*, 1099–8292.
22. Chang, C.H.; Chou, T.C.; Chen, W.C.; Niu, J.S.; Lin, K.W.; Cheng, S.Y.; Tsai, J.H.; Liu, W.C. Study of a WO_3 Thin Film Based Hydrogen Gas Sensor Decorated with Platinum Nanoparticles. *Sens. Actuators B Chem.* **2020**, *317*, 128145. [CrossRef]